J. S. Afr. Inst. Min. Metall., vol. 88, no. 12.
Dec. 1988. pp. 401-410.

Internal damping characteristics of a mine hoist cable undergoing non-planar transverse vibration

by R.R. MANKOWSKI*

SYNOPSIS

The work described in this paper is an attempt to increase present-day knowledge of fatigue in mine hoisting cables, particularly the internal energy loss arising from interwire/strand friction in a cable undergoing periodic non-planar transverse vibration. Such frictional energy loss is known to be one of the major influences limiting the useful working life of hoisting cables in use today, and is responsible for the large capital outlay required to maintain the high safety factors prescribed by the mining industry.

The experimental method employed identifies two mechanical characteristics of cables that are independent of amplitude and frequency, and are primarily attributed to the type of cable construction. Interest is focused on the time rate of change of curvature as the major parameter influencing the internal damping mechanism. Empirical results confirm that amplitude and mode number play an important role in quantifying the internal losses, and also reveal that a critical radius of curvature exists below which damage due to vibration fatigue rises exponentially to potentially high levels.

SAMEVATTING

Die werk beskryf in hierdie referaat is 'n poging om die teenswoordige kennis van vermoeidheid in mynboukabels, en veral die inwendige energieverlies as gevolg van tussendraad/stringwrywing in 'n kabel wat aan periodieke nieplanêre dwarsvibrasie onderhewig is, uit te brei. Dit is bekend dat sodanige wrywingsenergieverlies een van die belangrikste faktore is wat die nuttige werklewe van hyskabels wat tans gebruik word, beperk, en verantwoordelik is vir die groot kapitaaluitleg wat nodig is om die hoë veiligheidsfaktore wat deur die mynboubedryf voorgeskryf word, te handhaaf.

Die eksperimentele mode wat toegepas is, identifiseer twee meganiese eienskappe van kabels wat onafhanklik van amplitude en frekwensie is en in die eerste plek aan die tipe kabelkonstruksie toegeskryf word. Die belangstelling is toegespits op die tempo van krommingsverandering as die belangrikste parameter wat die inwendige dempmeganisme beïnvloed. Empiriese resultate bevestig dat amplitude en modusgetal 'n belangrike rol in die kwantifisering van die inwendige verliese speel en toon ook dat daar 'n kritieke krommingstraal bestaan waaronder skade as gevolg van vibrasievermoeidheid eksponensieel tot potensieel hoë vlakke styg.

INTRODUCTION

The problem of damage due to vibration fatigue continues to impose limits on winding velocities, depths of wind, and payloads in modern, deep South African gold mines. Until the mechanism of internal energy loss inherent in the transverse vibration of cables is thoroughly understood, such damage will continue to have a marked effect on the running costs and efficiency of South African mining operations.

Two major reasons impeding engineering breakthroughs in this area are the complex nature of the internal damping mechanism and the nonlinearity of the dynamic response of the cable to time-dependent boundary conditions. To date, a purely mathematical solution to the problem appears intractable, and it has become necessary to give increasingly more serious consideration to experimental results. Accordingly, the primary objective of the investigation described here was to determine experimentally (by laboratory simulation) the internal losses of a mine hoisting cable undergoing non-planar transverse vibration of large amplitude in the spectral neighbourhood of its fundamental and higher harmonic frequencies.

The scope of the investigation was limited to the mine geometries most likely to be encountered in practice in deep South African mining operations, namely the single-drum and the Blair multi-drum winding systems. The length of cable extending from the winding drum to the headsheave, commonly referred to as the catenary, suffers the most violent transverse vibration in practice, and hence served as the section of cable to be modelled in this investigation. The symbols used are defined at the end of the paper.

HISTORICAL NOTE

The groundwork on the fundamental and analytical aspects of the internal damping characteristics of structural cable and their influence on transverse vibration was conducted in the early 1950s by Yu[1]. The cable used was a 7-wire specimen (0,4 $kg \cdot m^{-1}$) formed by 6 helical wires stranded round a single-core wire. All the constituent wires were zinc-coated and of similar chemical composition, the nominal diameter being approximately 9,5 mm, the overall length 2000 mm, and the lay length 127,0 mm. Yu's investigation concentrated on the deter-

* Associate Professor, Department of Mechanical Engineering, University of Durban-Westville, Private Bag X54001, Durban 4000.

ISSN 0038-223X/$3.00. Paper received 29th June, 1988.

mination of hysteretic damping characteristics of a family of these specimens undergoing planar vibration in a state of zero tension.

Although the specifications and experimental method employed were distinctly far removed from the geometry and dynamic conditions of present-day mine hoisting cable, the following observations from that early investigation are relevant and describe the basic nature of the internal damping of stranded cable undergoing free planar vibration.

(1) The solid internal friction of the wire material is small.
(2) For practical purposes, it can be assumed that only dry friction exists (interstrand friction).
(3) The damping capacity (dissipation of energy per cycle) associated with internal dry friction is a linear function of amplitude.
(4) A critical amplitude seems to exist, above which the curve of specific damping capacity begins to rise hyperbolically.

In the past three decades, it appears that little independent research has carried Yu's pioneering efforts further in an attempt to expand present knowledge on the damping characteristics of mine hoisting cable. A number of investigations, however, have dealt with the static and dynamic response of massive guy cables. A detailed account of developments in this field is given by Davenport[2], in which he points out that Yu's conclusions clearly establish an equivalent viscous damping to be of the order of 2 to 7 per cent of critical damping. While this may be true for dry cables of simple geometry, its application to massive guy cables and mine hoisting cables is questionable on the grounds that these cables are much more complex in their construction: concentric left- and right-handed helices containing inner cores that deform in the plastic regions (polypropylene, sisal, and hemp impregnated with bitumen-based lubrication).

Simplified models of stranded cables employing a viscous damping mechanism proportional to velocity are decidedly more popular in the literature mainly because of the relative ease of formulation and solution. However, when the analyses account for tension gradients along the length of a cable in addition to internal structural damping proportional to amplitude and frequency, a nonlinear response manifests itself in the form of *drag-out* and *jump phenomena*[3]. These phenomena primarily describe the response of the medium to forced vibration of varying frequency passing through resonant conditions.

Vanderveldt[4] also cites the work of Yu[1], and adds that no simple model taking into account the transverse damping behaviour can be assumed. Furthermore, he contends that at least both the usual structural and viscous types of damping must be included in any analysis attempting to predict the attenuation of transverse waves that are propagated in a stranded cable. Vanderveldt[4] surmounted this mathematical difficulty by assuming a frequency-dependent coefficient of viscous damping. In this way, and providing the excitation is periodic, any other type of internal damping mechanism present is assumed to be contained in the damping coefficient. His theoretical and experimental results show particularly good agreement and, where relevant, are seen to complement Yu's experimental results as follows.

(a) For a metallic core, the internal damping is affected by the tensile load. (Radial forces and inter-strand stress increase with increasing axial tension so that dry-friction damping also shows an increase.)
(b) For non-metallic cores, the damping capacity increases as the axial loads decrease.

It is worth while mentioning here that, although Yu[1] commented on the dependence of damping on amplitude, neither Davenport[2] nor Vanderveldt[4] explicitly considered the effect of curvature and its time rate of change as a parameter influencing the dissipation of energy. The mathematical form of this parameter is given by Kolsky[5]: considering a plane distortional (bulk) wave that is propagated in the positive x direction with its particle motion in the y direction, the governing equation of motion can be shown to be

$$m\frac{\delta^2 y}{\delta t^2} = u\frac{\delta^2 y}{\delta x^2} + \hat{u}\frac{\delta}{\delta t}\left(\frac{\delta^2 y}{\delta t^2}\right), \quad \text{..... (1)}$$

with general solution

$$y = e^{-bx}\cos(x - Ct) \quad \text{..... (2)}$$

where b and C are both frequency-dependent, m is the mass density, u the shear modulus, and $\hat{u}$ the shear viscosity. Attention is drawn to the last term of Equation (1), which clearly associates the time rate of change of curvature with the shear viscosity.

PRELIMINARY DISCUSSION

In Fig. 1 the envelope of a length of cable undergoing free non-planar transverse vibration in the fundamental mode is shown over one complete cycle in increments of one-quarter periods. The length of the span is $2 \cdot L$ and the amplitude at mid-span is S. To within first-order terms, the mathematical curve traced out by the cable during vibration at any one instant can be approximated by a parabolic arc having its axis perpendicular to the chord joining the supports at the boundaries. This mathematical approximation of the curve, as pointed out by Dean[6], introduces errors that are small when the chord is horizontal and the sag-to-span ratio is less than 0,02. When the chord is not horizontal, symmetry is lost, and the cable will hang in the mathematical trace of a truncated catenary in its equilibrium position. However, for relatively small sag-to-span ratios, the approximation to a shallow parabolic arc is sufficiently accurate and does not introduce significant errors in the analysis. Parabolic-for-catenary approximations are frequent in the literature, particularly for the dynamic analysis of massive guy cables having inclined spans.

Boundary Conditions

When the diameter of the cable is large enough compared with the span, and the radius of curvature of the vibrating cable is sufficiently small, a local gradient in flexure stress will be set up in the cable. Depending on the type of boundary conditions, two gradients in flexure stress are possible: (i) a constant gradient and (ii) a time-dependent gradient varying with the mode of vibration. In the following analysis, both types of gradients are considered and are the result of ball-and-socket arrangements connecting the vibrating cables to the support, the types

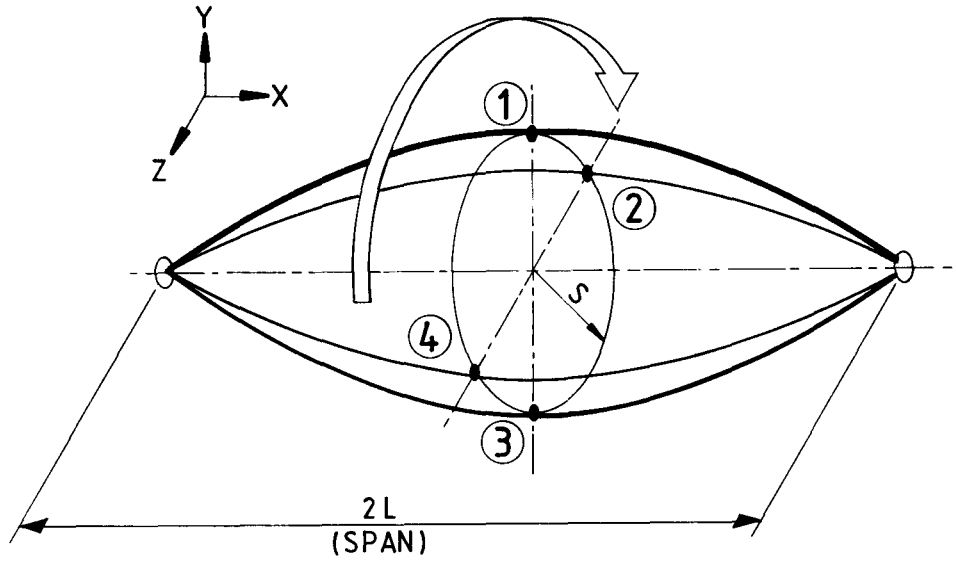

Fig. 1—Envelope of cable undergoing free non-planar transverse vibration in the fundamental mode

of rotational constraints imposed at the boundaries being the sole controlling influence on the gradients.

Constant Gradient in Flexure Stress

In this example the ball-and-socket joints are constrained in a manner that allows the cable to rotate about its geometric centre and revolve round the span (Fig. 2). Thus, the boundary conditions employed here allow the ball joints 3 degrees of rotational freedom within the sockets. This is tantamount to a rigid length of cable whirling round the span defined by the supports. Fig. 2 shows the circular orbit of a plane section of this cable occurring at mid-span in the y–z plane; the span here is taken normal to the page. The letter A is assumed fixed to the transverse section of cable, where, it is noted, the letter A revolves about the span *and* is seen to rotate about its geometric centre relative to an inertial reference fixed to the supports. The gradient in flexure stress occurring at the apex of the letter A is also shown in Fig. 2 and is seen to be constant for all time t. The indicators (C−) and (T+) in Fig. 2 represent the relative compressive and tensile states respectively occurring on the surface of the sections indicated as it continues its cycle.

From basic beam theory the flexure stress here is tensile owing to the fact that the apex remains at the outermost fibres of the circular section during vibration. The nature of the constraints also prevents the neutral axis (*NA*) from moving relative to the fixed indicator A. The constant value of the flexure stress in this example is attributed to centrifugal effects of the whirling cable combined with the bending effects.

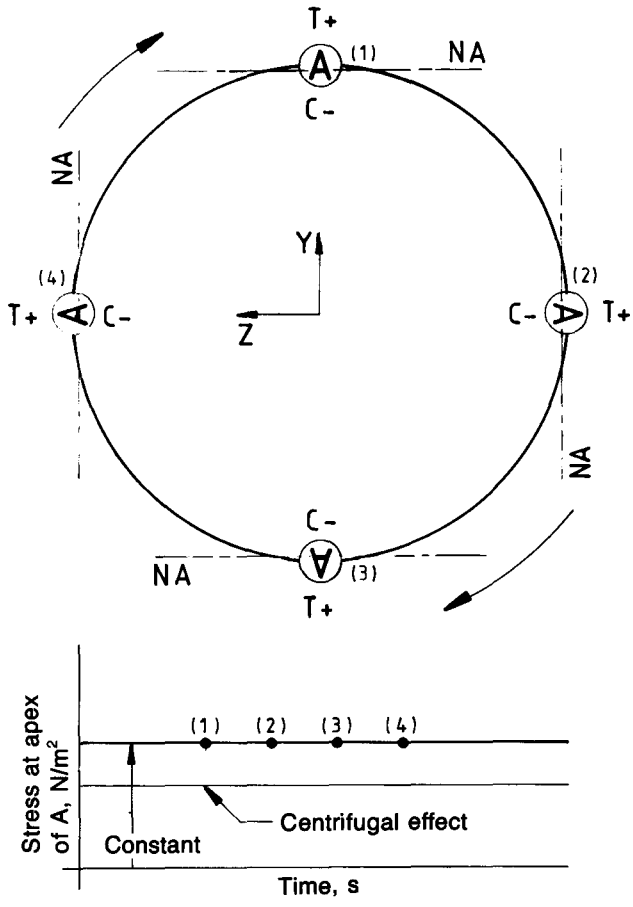

Fig. 2—Flexure stress occurring at a fixed point on the cable, rotational motion

Time-dependent Flexure Stress

The boundary conditions in this example are similar to those above with the exception that rotation about the X axis is constrained. As a consequence, the reference letter A, as shown in Fig. 3, now becomes irrotational. This fact is borne out by the unchanging vertical orientation of the letter A over one complete cycle. Furthermore, the reference of the apex of letter A experiences a flexure-stress cycle as it completes one revolution round the span. Noteworthy here is the time-dependent orientation of the neutral axis where it is seen to rotate relative to the fibres comprising the cable. The variation in flexure stress occurring at the apex of A is plotted against time over a period of two cycles in Fig. 3. Again, the constant component of tensile stress is attributed to the centrifugal effects arising from the increase in arc length as the cable balloons to a dynamically stable configuration.

Internal Energy Loss versus Boundary Conditions

In the former case of a vibrating cable having a fixed

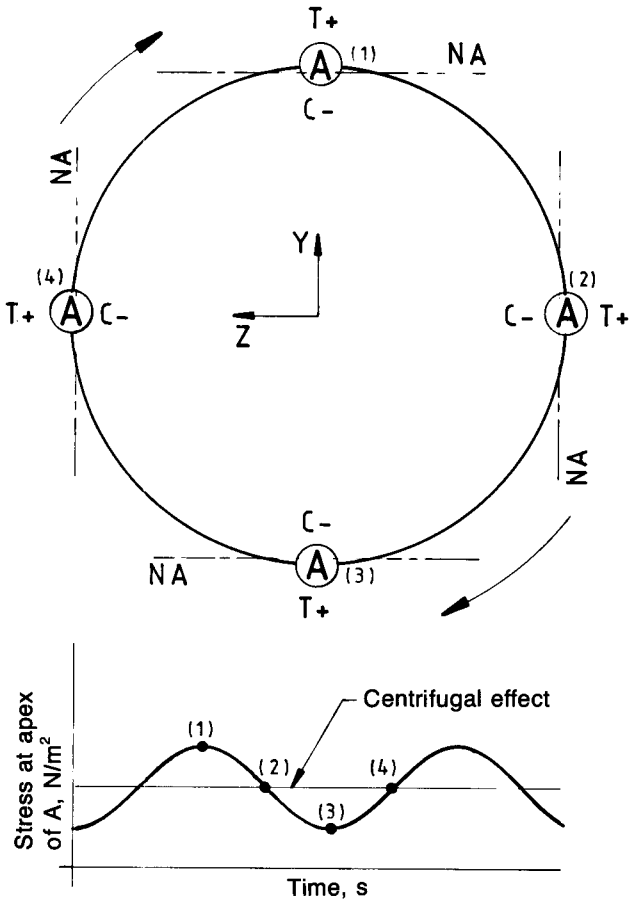

Fig. 3—Flexure stress occurring at a fixed point on the cable, irrotational motion

stress gradient, it becomes clear that no internal losses occur because there is no relative movement between adjacent layers or strands, nor is there any physical distortion of individual wires themselves. In the absence of aerodynamic damping, and of interstrand friction and frictional losses in the ball-and-socket joints, the cable in this instance (once set in motion) would continue to vibrate indefinitely.

The latter case, however, has much more practical appeal in that the study of irrotational motion is more prevalent in systems of vibrating cables and similar structures governed by the hyperbolic wave equation. Under these boundary conditions, it can be appreciated that all the fibres of the cable in the span area are cyclically sliding over or against adjacent fibres. The radial and normal components of flexural (bending) stress are clearly time-dependent and a function of the cable's orientation in space. Likewise, the shear-flow, and longitudinal and transverse shearing-stress components, are also dependent on the orientation. Moreover, as both of these complementary stresses are dependent on the radius of curvature, R, defined by the relation

$$\frac{E}{R} = \frac{M}{I} = \frac{\sigma}{y}, \quad \text{..... (3)}$$

the sag-to-span ratio or dynamically equivalent amplitude-to-span ratio and the frequency of vibration play an important role in governing the rate of internal energy loss.

The end physical result of the energy loss described above can generally be classified as transverse cable fatigue. Fatigue in this instance is manifest by worn individual wires accompanied by a general loss in their tensile strength as well as ductility. In the more severe cases of sustained violent vibration fatigue, individual broken wires are common-place. Modern *in situ* non-destructive testing techniques and periodic inspections, however, are quick to identify such damaged cables and alert the mining engineers of impending cable failure.

EXPERIMENTAL APPARATUS

The specifications of the mine cable used in this investigation were 43,5 mm (nominal diameter) with construction 6 × 32(14/12/6 tri)F and linear mass density 8,00 $kg \cdot m^{-1}$. In Fig. 4, a length of cable is shown suspended from supports of unequal height. The boundary conditions restricted the motion of the cable at the supports to pure rotation about the central longitudinal axis of the cable. Full thrust bearings were used for this purpose.

A predetermined tension and cable geometry were obtained by a hydraulic jack positioned at the lower end and locking devices fixed to the bearing casings at the lower and upper support ends. The movement of the jack and lower support were constrained to horizontal translation in the vertical plane defined by the suspended cable. The upper thrust bearing was hinged to accommodate any desired slope and, once the inclination of the upper bearing had been adjusted to match the slope of the cable, the bearing casing was locked into position. In this way, both thrust bearings were subject to purely axial thrust (tension) through their axial centres.

The suspended cable was excited by rotating the lower end by an electric motor, gear-reduction transmission, a series of chain drives, and a Reynold coupling. The Reynold coupling was situated between the driven end of the cable and the driving unit, and had the advantage of isolating the dynamic response of the cable from the excitation. This is desirable since mechanical feedback in the form of reflected longitudinal and transverse waves could (given sufficient build-up time) modulate the frequency and amplitude of the excitation, especially in the neighbourhood of resonant conditions.

The speed of the electric motor was controlled by a 3,7 kW three-phase variable-frequency driving unit, and monitored by an electro-optical revolution counter. The horizontal component of tension was measured by an in-line hydraulic transducer, which was situated behind the lower thrust bearing and rotated with the cable. The applied torque to the Reynold coupling was determined by a mechanical equivalent of a floating field dynamometer. The motor, transmission, and chain drives were housed in a single unit, which was mounted on trunnions and, under torque reaction, this unit could rotate about the trunnion bearings and be counterbalanced by movable masses. Thus, the relative movement of the balancing masses served as an indication of the applied torque.

To rid the central dynamometer carriage of its natural pendulum-type vibration, an extension arm fixed to the carriage was immersed in motor oil, the immersed sec-

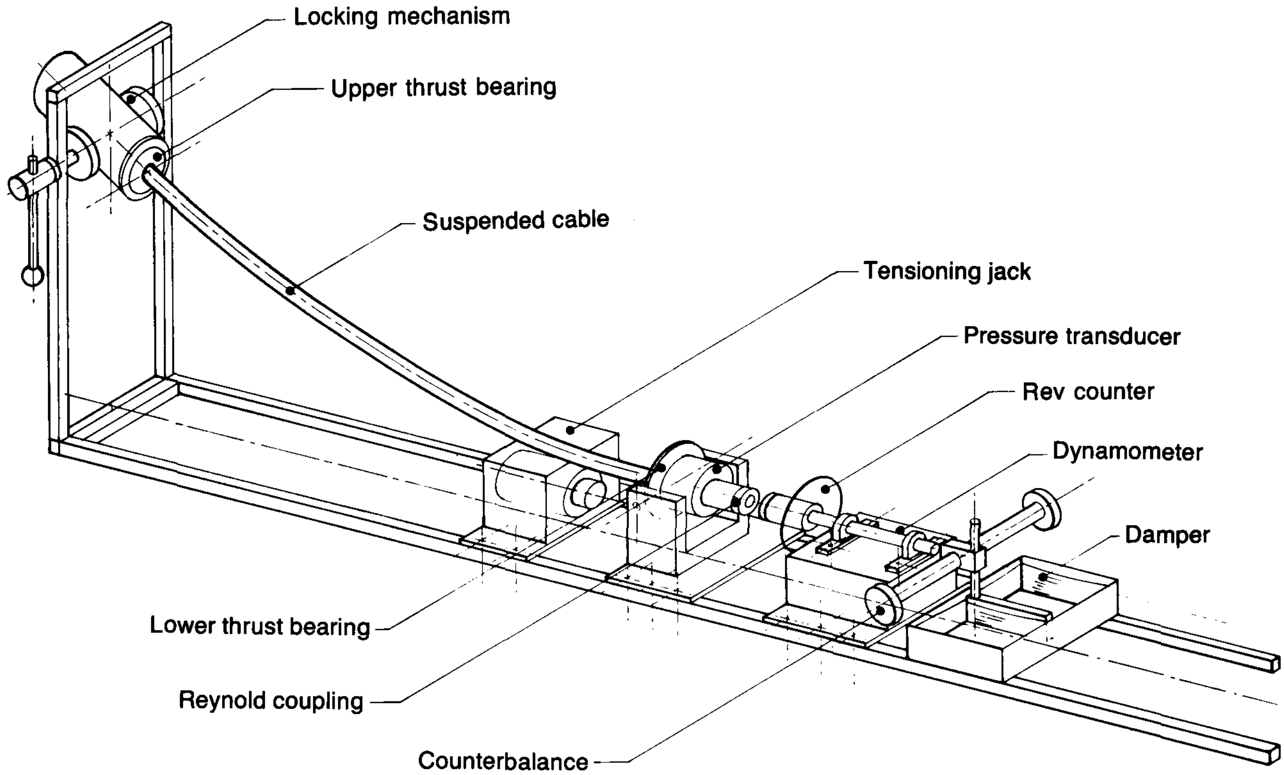

Fig. 4—Isometric sketch of the layout of the test apparatus

tion being a flat paddle placed normal to the direction of oscillation.

INTERPRETATION OF TORQUE MEASUREMENT

If the starting torque and subsequent first-order transient disturbances are discounted, the steady-state power delivered to the rotating cable per unit time, P_T, consists of

(1) the power required to overcome the rolling friction of the thrust bearings, P_B, and
(2) the power dissipated in the form of internal losses of the cable, P_C, arising from the continuous flexure cycle as the cable rotates about its centroidal axis, which is defined by the trace of its static equilibrium position.

It follows then that, per cycle,

$$P_C = P_T - P_B, \qquad (4)$$

where clearly $2 \cdot P_C$ represents the internal power loss associated with a length of the mine hoisting cable equal to twice the length of the laboratory model shown in Fig. 5. If this equivalence is carried a stage further, it can be seen that the power loss $2 \cdot P_C$ is mechanically equivalent to the internal power loss inherent in the system described in Fig. 1 and Fig. 3, in which a $2 \cdot L$ m length (span) of cable is undergoing irrotational non-planar transverse vibration in the fundamental mode with amplitude S and a frequency equal to the rotational frequency of the physical model. The physical justification for this equivalence lies in the fact that both systems undergo an identical flexure-stress cycle as a result of having the same time rate of change of curvature. This equivalence forms the basis of the experimental method described below.

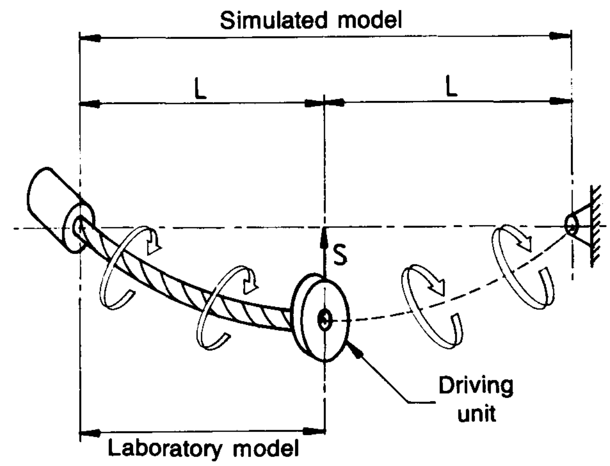

Fig. 5—Scope of the laboratory and simulated models

Thus, for an arbitrarily fixed sag-to-span ratio, $S \cdot L^{-1}$, and rotational frequency, F, of the physical model, it is possible by proper measurement to determine the internal power loss of an equivalent system undergoing irrotational non-planar transverse vibration at frequency F, amplitude S, and span length $2 \cdot L$.

EXPERIMENTAL PROCEDURE

The characteristics of the bearing loss were obtained from a 1 m length of horizontal cable tensioned between the thrust bearings. The tension, applied torque, and rotational frequency were recorded and tabulated to obtain the bearing-power loss for a particular set of control parameters. Under high tension, the short length of cable had a negligible sag-to-span ratio and insignificant weight. Thus, to all intents and purposes, the bearing characteristics recorded in this manner were represen-

tative of purely axial loads passing through the geometric centre of the bearings. A family of curves representative of the characteristics for four different rotational frequencies is shown in Fig. 6. Over the range of tension 2,0 to 20,0 kN, a linear relation between the parameters is evident. In the linear range, the ordinate difference is approximately 0,15 N-m per 15 r/min. As a matter of engineering interest, the thrust-bearing casings were removed from the front axles of a discarded Citroen DS Series 1974 model automobile.

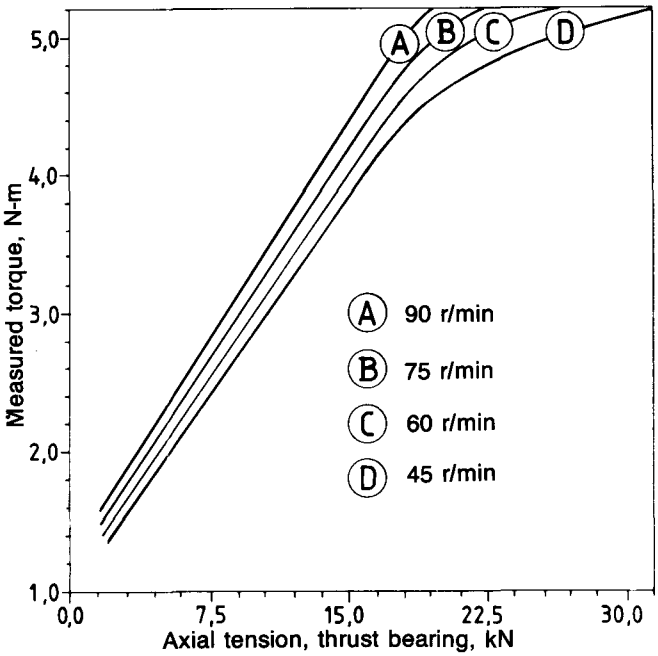

Fig. 6—Thrust-bearing characteristics

All the power calculations (loss and otherwise) are based on the general relation

$$P = 2\pi \cdot F \cdot T \text{ (W)}, \quad \ldots\ldots\ldots\ldots\ldots\ldots\ldots\ldots \quad (5)$$

where F (Hz) is the rotational frequency of the driven lower end and T (N-m) the torque measured on the dynamometer.

As the power required to overcome the internal friction of the driving unit for a particular torque and driving frequency is common to both the P_T and P_B measurements, the cable power loss, P_C, is seen to be independent of frictional losses in the driving unit. This is made clear by the right-hand side of Equation (4).

Initially, a length of cable approximately 20 m long was locked between the bearings under zero tension and supported in a horizontal position (zero sag). This ensured that the stress gradient was uniform before the cable was locked into the supports. After the cable had been locked in the thrust bearings in this manner, the undriven end was raised to a sag distance of 1,52 m. For this configuration, four sets of torque measurements were taken for rotational frequencies of 45, 60, 75, and 90 r/min. The undriven support was then progressively lowered to 0,92 m, 0,62 m, and finally 0,32 m. At each different sag setting, the torque measurements were taken again for the four rotational frequencies. Thus, for the 20 m length of cable, the torque measurements over a range of sag-to-span ratios 0,076, 0,046, 0,031, and 0,016 were obtained. This resulted in 16 sets of results being recorded for this single cable configuration.

The above procedure was repeated for progressively shorter lengths of cable, lengths of 1 m being threaded through the upper support bearing, cut, and removed. This procedure continued until an approximate 6 m length remained for testing. A second cable (again approximately 20 m) was tested in an identical manner. This afforded greater accuracy (more data points) and a check on the reproducibility of the results.

It was noticed during the early stages of testing that the torque measurement drifted monotonically when a single cable configuration was tested for periods lasting more than 10 to 15 minutes. The amount of drift was seen to be frequency-dependent and was attributed to the build-up of heat arising from the internal-friction mechanism mentioned earlier. In addition, continuous excitation caused the thrust bearings to change their characteristics because of a decrease in the viscosity of the bearing lubrication resulting from an increase in the frictional heat within the bearing casings themselves. In order to eliminate this undesirable aspect from becoming another variable in the experimental method, it was judged necessary to excite a particular cable configuration for not more than 10 seconds with sufficient lapsed time between readings. An added advantage of the short-burst testing was that potentially disruptive dynamic conditions occurring near or at resonance were eliminated. This approach proved successful in giving a high degree of reproducibility over the spread of collected data.

RESULTS

Fig. 7 is a graphical representation of all the results from the 90 series of tests conducted at 90 r/min. The laminar slices correspond to data collected for cable sags 0,32, 0,62, 0,92, and 1,52 m. The upper portion of each slice is the loci of the total measured torque for the testing of the various suspended cables. For example, in Fig. 7, for a configuration having a sag-to-span ratio of 0,04, a sag of 0,32 m, and an excitation frequency of 90 r/min, the measured torque is seen to be 3,2 N-m. The lower portion of each slice represents the drag in thrust-bearing torque at the excitation frequency of 90 r/min. The ordinate value of the drag in bearing torque is obtained from the tabulated results of Fig. 6. For example, given a sag-to-span ratio of 0,04, a sag of 0,32 m, and a tension of 8,1 kN recorded from the experiment, the torque drag is obtained directly from curve A, and in this instance 8,1 kN is correlated with a drag in bearing torque of 2,95 N-m. In Fig. 7, the difference between the upper and lower ordinates for a given sag is a measure of the energy required to overcome the internal friction at 90 r/min. Thus, in the present discussion, (3,20 – 2,95) N-m or 0,25 J, are lost in the form of internal friction. At a rotational frequency of 90 r/min (1,5 Hz), this is equivalent to a power loss of 2,35 W.

Fig. 8 is a version of Fig. 7 in which the thrust-bearing loss is suppressed to zero and the relative ordinate distance to the total measured torque of the suspended cable is preserved and converted to a power loss. The final reduced results of the tests at 45, 60, and 75 r/min are also shown. Of particular interest is the linear relationship between the power loss and the frequency.

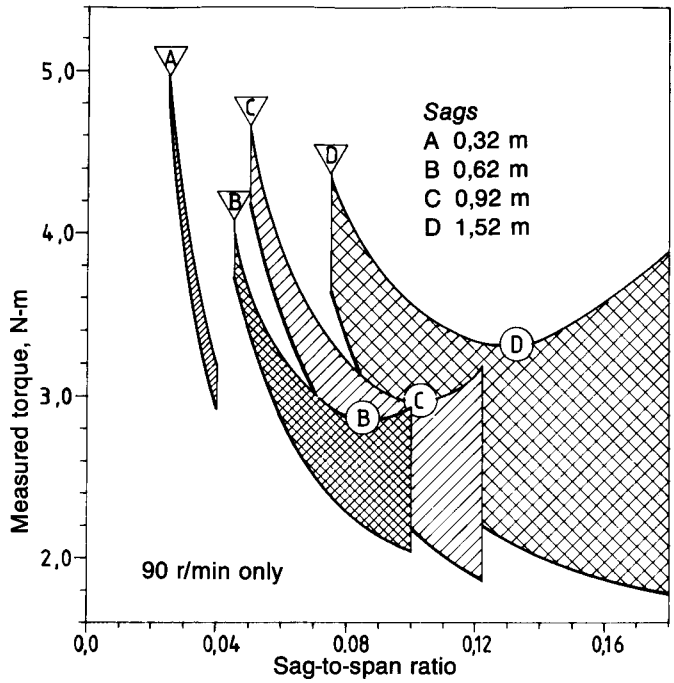

Fig. 7—Energy levels (the upper traces indicate total measured torque, and the lower traces indicate bearing loss)

DISCUSSION OF RESULTS

The upper traces in Fig. 7 show three distinct minimum values of energy for increasing values of sag-to-span ratio. For the test specimen having a sag of 0,62 m, the minimum energy level occurs at a sag-to-span ratio of 0,085; likewise for the specimen having a sag of 0,92 m, the minimum occurs at 0,103 and, for the 1,52 m sag, at 0,133. For sag-to-span ratios larger than these critical values, the energy levels are seen to rise exponentially. This is particularly evident in Fig. 8 where, beyond a sag-to-span ratio of 0,133, the internal cable loss rises dramatically for the test specimen having a sag of 1,52 m.

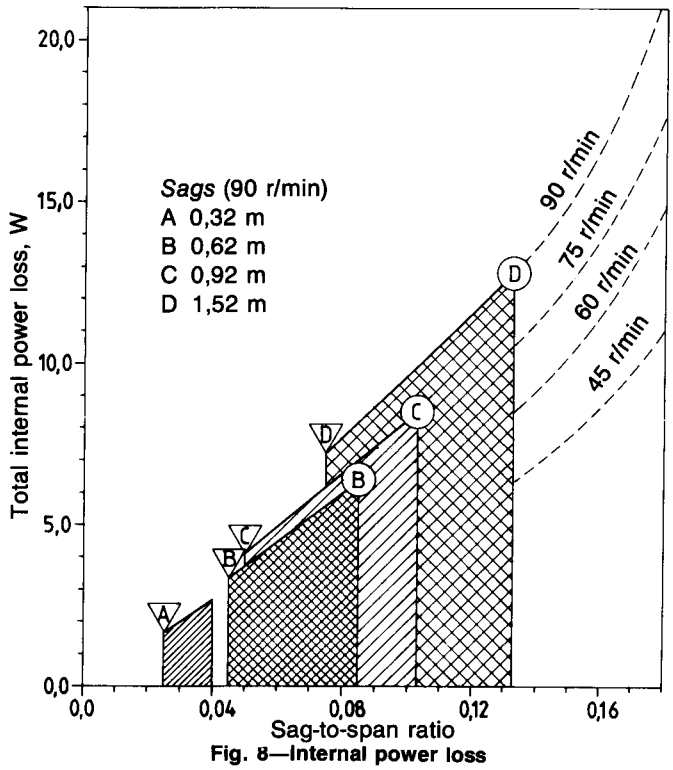

Fig. 8—Internal power loss

If the mathematical traces of the specimens used to determine the data presented in Fig. 7 are parabolic and of the form

$$Y = kX^2, \quad \ldots\ldots\ldots\ldots\ldots\ldots\ldots\ldots\ldots\ldots \quad (6)$$

three equations can be written for the critical cable configurations that generate the relative minimum energy levels or critical points. For convenience in future discussion, the sag-to-span ratio is hereafter abbreviated to SSR.

Sag 0,62 m
Span 7,29 m
SSR 0,085

$$0{,}62 = k(7{,}29)^2: \; k = 0{,}0116\ \text{m}^{-1}$$

Sag 0,92 m
Span 8,93 m
SSR 0,103

$$0{,}920 = k(8{,}93)^2: \; k = 0{,}0115\ \text{m}^{-1}$$

Sag 1,52 m
Span 11,43 m
SSR 0,133

$$1{,}52 = k(11{,}43)^2: \; \frac{k = 0{,}0116\ \text{m}^{-1}}{k_{AV} = 0{,}0116\ \text{m}^{-1}}.$$

The average value, k_{AV}, can now be used to determine the critical radius of curvature, R_{CRIT}, below which the internal energy loss rises exponentially. From the calculus,

$$R_{CRIT} = (2k_{AV})^{-1} = 43{,}00\ \text{m}. \quad \ldots\ldots\ldots\ldots\ldots \quad (7)$$

Fig. 9 shows a fitted curve for the loci of sags as a function of the critical SSRs. The point on the curve representing the critical SSR for a sag of 0,32 m was obtained from the derived value of k_{AV} above. It is noted, for all points below the fitted curve, that the radius of curvature is less than 43,00 m and the power loss in this region rises exponentially for increasing SSR. For points above the curve, the radius of curvature is greater than 43,00 m, and the internal power loss rises in a linear fashion as shown in Fig. 8. It is noteworthy that these results qualitatively bear out points (3) and (4) mentioned earlier in this paper. Yu[1] attributes the existence of a critical radius of curvature (critical amplitude) to the tightening of the cable as the cable is bent from its neutral position and the contact surface between the wire increases. Furthermore, he contends that the critical radius of curvature is the radius at which uniform contact of wire surfaces in the strands has been reached.

An empirical relation can be derived from the family of curves shown in Fig. 8. The internal power loss arising as a function of the dependent variables SSR, F, and the sag is given here as

$$P_{LOSS} = SSR \cdot F \cdot 42{,}75(1{,}0 + 0{,}34sag)\ \text{W}. \quad \ldots\ldots \quad (8)$$

The set of all possible values of SSR and sag for which Equation (8) is valid is limited to the range of values shown above the curve in Fig. 9. Thus, Equation (8) is applicable only over the range of values for which the internal power loss remains linear as defined by the 'Linear rise' region in Fig. 9.

As mentioned earlier, the internal power loss of a cable system undergoing non-planar transverse vibration in the fundamental mode can be obtained if the results of Equa-

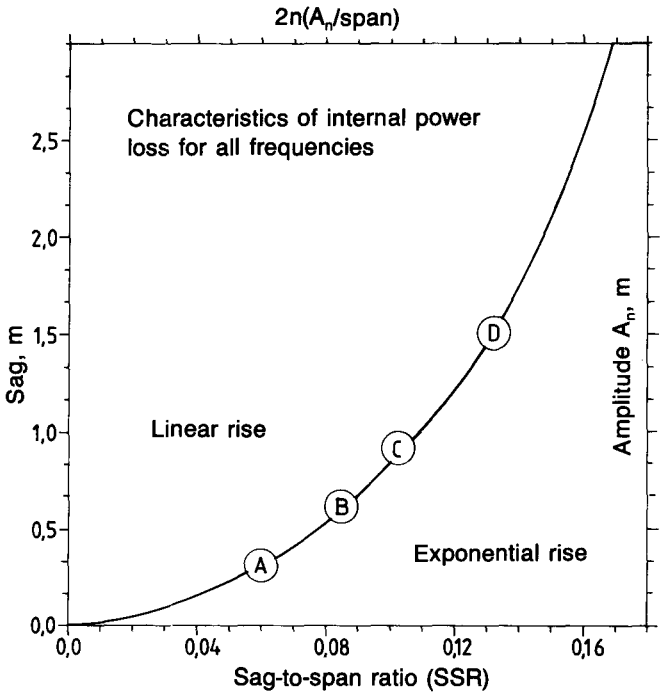

Fig. 9—Loci of critical sag-to-span ratios

tion (8) are multiplied by a factor of 2. This is clarified in Fig. 10(a), where the dynamic and physical properties of the laboratory model are embedded in a simulated vibrating system experiencing twice the internal power loss. Of particular note in the simulated model is the distance between the support points shown here as $2 \cdot L$. Similarly, Fig. 10(b) shows the equivalence between the laboratory model and a simulated model vibrating in the second mode. The distance between the supports in the simulated model shown here is $4 \cdot L$, and the internal power loss is 4 times that of the laboratory model. Lastly, reference to Fig. 10(c) shows the equivalence between the laboratory model and a simulated model vibrating in the third mode. The loss and the span distance of the simulated model are shown to be 6 times those of the laboratory model.

Obviously, the term *sag-to-span ratio* as used conventionally in the literature poses some degree of difficulty

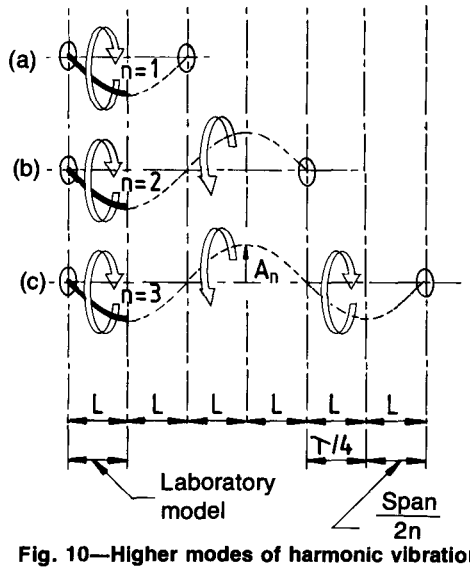

Fig. 10—Higher modes of harmonic vibration

in interpretation, especially when applied to the analysis of higher modes of vibration. To obviate any risk of misunderstanding, the term *span* will hereafter refer to the straight-line distance between the end supports of a vibrating cable independent of the mode of vibration. This interpretation of *span*, coupled with the discussion above concerning the internal power-loss equivalence, results in the final form of the expected internal power loss of a simulated cable system vibrating in any of the harmonic modes as

$$P(n)_{LOSS} = (2n)SSR \cdot F_n \cdot C_1(1,0 + C_2A_n) \text{ W}, \quad \ldots\ldots (9)$$

where

n is the mode number,
$P(n)$ is the internal power loss for the n^{th} mode,
A_n is the amplitude of vibration of the n^{th} mode (m),
F_n is the frequency of vibration,
SSR is now redefined as $2n \cdot A_n$/span,
C_1 is the damping capacity (J), and
C_2 is the curvature characteristic (m^{-1}).

For the cable in this investigation C_1 was determined experimentally as 42,75 J and C_2 as 0,34 m^{-1}. A precise physical interpretation of SSR as defined above can be given as the ratio of the amplitude A_n to the quarter wave-length (span/2n) of the standing wave set up on the cable.

Application to Kloof Gold Mine

The present investigation is part of an ongoing research project initiated in the early 1970s at the Chamber of Mines Research Laboratories, Johannesburg. The majority of research publications[3,7-9] resulting from these continuing efforts used on-site data collected from Kloof Gold Mine as source material. As the present author is familiar with the geometry, frequencies, and amplitudes of transverse vibration occurring at that Mine, it is thought a worth while exercise to close this paper with an analysis of the internal power losses in a single cable of the Blair double-drum winding system installed in the No. 1 Shaft at that Mine. A resonant condition occurring during normal operations is chosen for discussion, i.e. when the natural transverse frequency of the cable (catenary) extending from the drum to the headsheave is an integral multiple of the Lebus liner cross-over frequency at the winding drum. For purposes of discussion, worst-case amplitudes are used.

Data Applying to No. 1 Shaft

The following data apply to No. 1 Shaft.

C_1, C_2: The physical properties of the cable employed at Kloof are cable construction 6 × 30(12/12/6 tri)F and linear mass density 8,49 kg·m^{-1}. The geometry and density of that cable are not too dissimilar to the properties of the cable used in the investigation described in this paper. For this reason only, the cable characteristics C_1 and C_2 are assumed to take on the values 42,75 J and 0,34 m^{-1} respectively.

Span: Drum to headsheave distance 75,00 m

F_n: Fundamental drum frequency 1,12 Hz

A_n: Amplitude, fundamental mode A_1 = 2,0 m, n = 1, F_1 = 1,12 Hz
Range check: A_n and $2n(A_n/span)$ lie in the 'Linear rise' region of Fig. 9
Amplitude, second mode A_2 = 1,15 m, n = 2, F_2 = 2,24 Hz
Range check: Parameters lie in the 'Linear rise' zone
Amplitude, third mode A_3 = 1,0 m, n = 3, F_3 = 3,36 Hz
Range check: Parameters lie in the 'Linear rise' zone
Amplitude, fourth mode A_4 = 0,75 m, n = 4, F_4 = 4,48 Hz
Range check: Parameters approach critical loci.

Calculations of Internal Power Loss

The use of Equation (9) and the mode parameters given above as inputs results in the following power losses:

$P(1)$ = 7,60
$P(2)$ = 46,27
$P(3)$ = 92,30
$P(4)$ = 171,80 W.

At first glance, these values appear insignificant and to some engineers perhaps not even worthy of consideration. This is certainly true when they are compared with the 6300 kW d.c. motor assemblies that drive the winding drums. However, taking into account that damage due to cable fatigue is an irreversible phenomenon lasting over an average of 75 000 trips per cable, serious consideration must be directed to the relative orders of magnitude between the losses in modal power and the cumulative effect they may have in limiting the working life of the cable.

CONCLUSION

The use of an empirical approach in this investigation gave rise to a highly comprehensive and efficient technique for quantifying the complex damping mechanism occurring in mine hoisting cables undergoing non-planar transverse vibration in all the harmonic modes. In the author's experience to date, neither theoretical nor experimental evidence based on the (irrotational–rotational) mechanical equivalence has been encountered in the literature. Because the basis of the method lies in the testing of the actual cable whose internal frictional characteristics are sought, any cable having suitable laboratory dimensions can be subjected to the dynamic test described here.

Two flexural-type damping characteristics were identified by an experimental method. The precise form that the damping took was dictated mainly by convenience in computation. It is, however, consistent with the damping encountered in analogous systems, and conforms qualitively to a type of shear-viscosity damping, or one that is proportional to the time rate of change of curvature. In the absence of a large body of concrete information on the exact nature of damping in this situation, the type of damping characteristics identified are justified: they have the virtue by being simple and ensure that a quantitatively correct assessment of the internal power loss is achieved.

It should be emphasized that the following conclusions are based on the testing of the dynamic response of a single mine hoisting cable of fixed construction. As a result, there may be some difficulties in the application of the following observations to other mine hoisting cables having different geometric construction. However, in spite of these potential differences, certain qualitative trends can be generalized and summarized as follows.

(1) The internal power loss of a mine hoisting cable can be characterized qualitatively and quantitatively by two experimentally determined parameters: a damping capacity coefficient, C_1, and a curvature characteristic, C_2. A mathematical relationship was developed that makes it possible, given these two coefficients and the dynamic environment of the cable (amplitude, span, and frequency), to assess the amount of internal power loss.
(2) A critical radius of curvature exists above which the internal power loss increases linearly with increasing amplitude-to-span ratio. Experimental evidence also shows the losses in this linear region to increase as the square of the mode number of vibration.
(3) For radii of curvature below the critical value, the internal losses rise exponentially, and no attempt was made to investigate the losses occurring in that region.
(4) For typical mine installations, the higher modes of non-planar transverse vibration have a significant influence on the undesirable effects associated with damage from vibration fatigue. This observation is based on the application of the empirical results obtained here to the dynamic conditions of an existing gold mine.

PROPOSAL FOR FUTURE RESEARCH

A variety of critical questions surfaced during the investigation, the most relevant being those relating to the unknown behaviour of cables differently constructed from the single cable used in the analysis. Further research could well take into consideration the factors that may influence the damping capacity and curvature characteristics of the various types of mine hoisting cables in use today. Briefly, the following factors thought to be of prime importance in this regard are the effects of

(1) lay length,
(2) number of constituent wires composing the strands,
(3) the various types of strand construction: round, triangular, non-spin, and locked coil,
(4) the physical properties of the core material, and
(5) bitumastic-based cable lubricants.

An appraisal of the five points above leads to the tantalizing question: Does a functional relationship exist between the damping characteristics (C_1 and C_2 as defined in this paper) and the well-documented expected fatigue-life cycles of the various types of mine hoist cables in use today? The author believes a relationship does exist, and a well-coordinated investigation into this area should have exciting practical and financial implications for the mining industry.

The experimental technique and testing apparatus developed in the Mechanical Engineering Laboratories at the University of Durban–Westville have proved to be accurate and reliable, and with the necessary modifications can provide information on the internal damping